Palaeoclimatic changes in Kveithola, Svalbard, during the Late Pleistocene deglaciation and Holocene: Evidences from microfossil and sedimentary records

Katia Carbonara [a,*], Karin Mezgec [b], Gabriella Varagona [c], Maria Elena Musco [b], Renata Giulia Lucchi [d], Giuliana Villa [a], Caterina Morigi [e,f], Romana Melis [c], Mauro Caffau [d]

[a] Department of Physics and Earth Sciences, Università di Parma, 43124 Parma, Italy
[b] Department of Physical Sciences, Earth and Environment, Università di Siena, 53100 Siena, Italy
[c] Department of Mathematics and Geosciences, Università di Trieste, 34128 Trieste, Italy
[d] OGS (Istituto Nazionale di Oceanografia e di Geofisica Sperimentale), 34010 Sgonico, TS, Italy
[e] GEUS (Stratigraphy Department Geological Survey of Denmark and Greenland), 1350 Copenhagen, Denmark
[f] Department of Earth Sciences, Università di Pisa, 56126 Pisa, Italy

ARTICLE INFO

Accepted 5 October 2016

Keywords:
Palaeoclimate
Arctic sediment core
Microfossils
Holocene
Late Pleistocene
Clay minerals

ABSTRACT

Climate changes are reflected in the Arctic ecosystem history over different timescales. We use a multi proxy-based approach for palaeoenvironmental and palaeoclimatic reconstructions, conducted on sediment cores, compared with summer insolation and Greenland ice core $\delta^{18}O$ data in order to establish a framework for climate changes from Late Pleistocene to late Holocene. Our dataset includes the results compiled from a sediment core, collected on the middle slope of the Kveithola Trough Mouth Fan (South of Svalbard) during the CORIBAR cruise (2013). The studied core presents remarkable lithological and magnetic susceptibility similarities with cores recovered in the same area during the SVAIS (2007) and the OGS-EGLACOM cruise (2008), allowing the construction of the age model. The results indicate that during the last 14.5 cal ky BP advances and retreats of the Svalbard Barents Sea Ice Sheet were strictly linked to the interplay of Atlantic and Arctic water inflows to the study area. During the deglaciation, from the Last Glacial Maximum to the onset of the Holocene, the climate underwent a series of abrupt changes including the Bølling-Allerød warm interstadial and the Younger Dryas cold event. During the early Holocene, the investigated area was dominated by enhanced warm Atlantic water inflow, which was concomitant with summer insolation increase, characterizing the Holocene Thermal Maximum. Conversely, the late Holocene was governed by deteriorating climatic conditions, with predominant Arctic/Polar water inflow on the surface water masses off Western Svalbard, possibly associated with summer insolation decline due to orbital forcing.

1. Introduction

The polar oceans are sites of deep-water formation driving the thermohaline circulation and affecting climate on a global scale. Palaeoclimatic reconstructions can be achieved through proxies, such as microfossil assemblages and clay mineral distribution, that provide key information for water masses provenance and environmental targets such as sea surface temperature (SST), salinity, sea-ice cover and marine biological productivity.

Here we focus on the marine biotic response to Late Pleistocene and Holocene climate changes, using an integrated approach on a sediment core. The aim of the present research is the reconstruction of the palaeoclimatic and palaeoenvironmental changes in the Kveithola glacial trough system (South of Svalbard) during the Late Pleistocene deglaciation and the Holocene on the basis of the microfossil phyto and zooplankton assemblages and clay mineral distribution. The Late Pleistocene deglaciation was an unsteady process; ice sheets, at various times, temporarily arrested, advanced and/or retreated affecting the climate of the surrounding areas. According to Winsborrow et al. (2010) the deglaciation of the SW Barents Sea (Bjørnøyrenna glacial trough system) initiated at ca. 15.5 cal ka BP, while Jessen et al. (2010) and Lucchi et al. (2013) indicated deglaciation on the NW Barents Sea started at ca. 20.5 cal ka BP. The subsequent Holocene is the youngest phase of the Earth climate history that began when the last glaciation ended. During the Quaternary, commonly preserved microfossil groups in polar areas include calcareous nannofossils (Backman et al., 2009), diatoms (Koç and Schrader, 1990) and planktonic foraminifera (Wollenburg and

* Corresponding author.
E-mail address: katia.carbonara@studenti.unipr.it (K. Carbonara).

Kuhnt, 2000). The distribution of these microfossils has been investigated in a sediment core, collected from the Kveithola Trough Mouth Fan (TMF) middle slope in the framework of the international project CORIBAR, sharing objectives with the International Polar Year (IPY) Activity 367 NICESTREAMS (Neogene Ice Streams and Sedimentary Processes on High-Latitude Continental Margins). The results from the studied core were compared with the dataset obtained from neighbouring sediment cores recovered during IPY 2007–2009: the SVAIS project (Development of an Arctic ice stream-dominated sedimentary system: The Southern Svalbard continental margin), funded as Spanish IPY research program, and the EGLACOM project (Evolution of a glacial Arctic continental margin: The Southern Svalbard ice stream-dominated sedimentary system), funded by the Istituto Nazionale di Oceanografia e di Geofisica Sperimentale (OGS), as contribution to IPY Italian activity.

The study of the Kveithola represents an excellent opportunity to improve the understanding of palaeoclimate variations over the approximately last 14.5 cal ky BP, because of the presence of an expanded and continuous sedimentary sequence from the last deglaciation to the Holocene. Past climatic reversals had major impacts on Arctic regions over timescales much shorter than orbital cycles and they provide a unique framework for today's climatic changes.

2. Study area

The Kveithola Trough Mouth Fan (TMF) is situated North-West of the Bjørnøya island and South of the Spitsbergenbanken, the shallowest bank in the Barents Sea having a water depth of 30–80 mbsl (Rüther et al., 2012) (Fig. 1a). The Kveithola is a glacial U-shaped trough with an East-West orientation and it is about 90 km long, 15 km wide, with a water depth that ranges between 200 and 400 mbsl (Rebesco et al., 2011; Rüther et al., 2012). The Kveithola, part of the Storfjorden glacial system, was carved by ice streams that during the last glacial period drained ice from both Svalbard, located in the Northern area, and Bjørnøya, located in the Southern area (Andreassen et al., 2008; Rebesco et al., 2011). The Storfjorden-Kveithola palaeo-ice stream is a small system compared to the major drainage systems of the Barents Sea (Svendsen et al., 2004); however, it contains a valuable high-resolution sedimentary and climate archive for its location close to the Fram Strait that represents the only deep-sea gateway for water masses exchange between the Arctic Ocean and the Greenland-Norwegian Sea. Two main currents interact in the study area: the West Spitsbergen Current (WSC) and the Eastern Spitsbergen Current (ESC) (Fig. 1b). At about 70°N the Norwegian Atlantic Current (NwAC) splits into the North Cape Current (NCaC), that flows into the Southern part of the Barents Sea, and the West Spitsbergen Current (WSC), that carries on Northward along the Western slope of Svalbard into the Arctic Ocean (Blindheim and Rey, 2004; Groot et al., 2014). The WSC transports relatively warm (6 to 8 °C) and salty (35.1 to 35.3‰) Atlantic water, keeping this area free of ice year-round (Aagaard et al., 1987). A branch of the WSC mixes with Polar water moving North of Svalbard and enters again the Barents Sea East of Spitsbergen. This current, the Eastern Spitsbergen Current (ESC), is characterized by lower temperature (0 °C) and salinity (34.3–34.8‰) with respect to the WSC being covered by seasonal sea-ice during winter that causes dense deep water formation by brine rejection (Loeng, 1991). The extent of the sea-ice cover is controlled by the Polar and Atlantic surface water boundaries, that constrain the location of the two oceanic fronts, the Polar front (PF) and the Arctic front (AF) (Fig. 1b). The PF corresponds to the average summer sea-ice margin and the AF is associated with the maximum extension of sea-ice during winter (Zamelczyk et al., 2012).

3. Material and methods

This study is based on the investigation of a 974 cm long gravity core (GeoB17603-3, in the following indicated as 17603-3) recovered on the

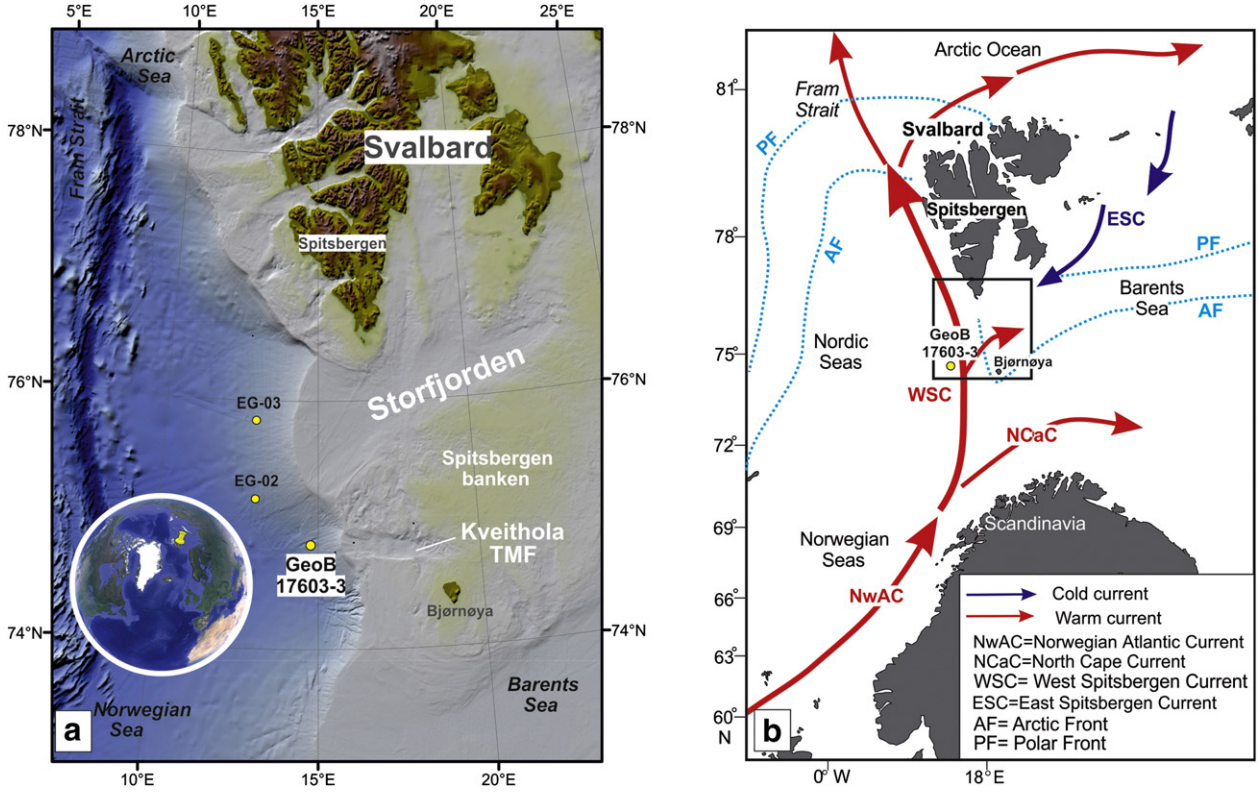

Fig. 1. a – Location of the study area. Yellow dots indicate the studied core CORIBAR 17603-3 and other cores also discussed in the text (EGLACOM cores); TMF = Trough Mouth Fan; b – oceanographic circulation in the NW Barents Sea. The black box indicates location of the study area.

Table 1
Core location, water depth and total sediment recovery for core 17603-3. TMF = Trough Mouth Fan.

Core ID	Lat. N	Long. E	Water depth (m)	Location	Total recovery (cm)
GeoB17603-3	74° 51,00′	14° 48,09′	1430	Middle slope of Kveithola TMF	974

Kveithola TMF middle slope during the CORIBAR cruise on board the R/V Maria S. Merian (summer 2013) (Table 1, Fig. 1a). The core was initially analysed using a GEOTEK Multi-sensor Core Logger for Magnetic Susceptibility (k), opened and visually logged. Sediment samples were collected regularly at 10 cm intervals and analysed for sedimentological characteristics and microfossil content, including calcareous nannofossils, diatoms and planktonic foraminifera.

3.1. Sedimentary analyses

A total of 29 samples were analysed for water content and grain size characteristics using a coulter counter laser Beckman LS-230 to measure the 0.04–2000 μm fraction at 0.004 μm resolution. The samples were initially treated with diluted peroxide and the disaggregated sediments were re-suspended into a 0.1% sodium-hexametaphosphate solution and left for 3 min in ultrasonic bath prior to measurement. The results were classified according to Friedman and Sanders (1978) grain-size scale.

Clay mineral analyses were performed on 29 samples at 30–40 cm sampling interval. Separation of the clay fraction was obtained by centrifugation during 1 min at 1050 rounds/min to settle the particles 2–63 μm (silt), and 10 min at 3980 rounds/min to settle the clay fraction leaving the pore water salt in suspension within distilled water.

X-ray diffraction (XRD) was performed on the clay samples mounted on smear slides, using a Philips PW1710 powder diffraction system, using CuKα radiation (40 kV, 40 mA). Each sample was analysed between 2° and 40° 2θ, with a step size of 0.02° 2θ in the air-dry state and after ethylene glycol solvation that permits the expansion of smectite peak to a basal spacing of about 17 Å. A slower scan, between 23° and 25.5° 2θ, with a step size of 0.005° 2θ was performed on the glycolated samples, in order to obtain a better resolution of the chlorite-kaolinite twin peak. Semi-quantitatively estimation of the main clay mineral abundance (smectite, chlorite, kaolinite and illite) was determined using the MacDiff software, relative percentages of each clay mineral were computed using weighting factors (Biscaye, 1965). Clay mineral percentage standard deviations were calculated using illite ±1%, smectite ±1%, chlorite ±2.5%, kaolinite ±2% according to Damiani et al. (2006).

X-ray fluorescence (XRF) core-scan analyses were performed at 1 cm resolution using an Avaatech instrument at 10 and 50 kV setting and the Ca, Fe and Ti contents were determined.

3.2. Chronology

Ten Accelerator Mass Spectrometry (AMS) ^{14}C ages were performed on planktonic foraminifera at NOSAM Laboratory (Table 2). The radiocarbon ages were calibrated with the software Calib 7.1 (Stuiver and Reimer, 1993) using the Marine13 calibration curve (Reimer, 2013) and applying an average marine regional reservoir effect $\Delta R = 67 \pm 34$ years, obtained from the Marine Reservoir Correction Database of Calib 7.1 for the North-Western Barents Sea area (Mangerud and Gulliksen, 1975; Mangerud et al., 2006). Calibrated ages at $\pm 1\sigma$ and $\pm 2\sigma$ are delivered by the program normalized to calendar year and are indicated in the following as cal a BP or as cal ka BP.

The age model for core 17603-3 is based on magnetic susceptibility correlations with two previously studied sediment cores (Fig. 2), located in the surrounding area, following the procedure described in Sagnotti et al. (2011), in which the radiometric ages from the EGLACOM cores EG-02 and EG-03 were transferred to a common stratigraphic depth on core 17603-3. Refining of the age model of core 17603-3 was assisted by the new radiocarbon dates. The lithological sequence and the magnetic susceptibility are consistent between the CORIBAR and EGLACOM cores and, for this reason, the upper part of the core 17603-3 was correlated to the Holocene sequence of core EG-03, whereas the lower part of the core was correlated to the post LGM sequence recovered in core EG-02. Down core ages were obtained by linear interpolation between dated/correlated levels (Fig. 2). Sediment accumulation rate was also determined (Fig. 3).

3.3. Micropalaeontological analyses

3.3.1. Calcareous nannofossils

A total of 98 samples were analysed for calcareous nannofossil content with a sampling interval of 10 cm. All samples were prepared from unprocessed material as smear slides, following standard techniques (Bown and Young, 1998) and examined using a Zeiss Axioskop light microscope at 1250× magnification. The coccoliths were counted in 200 fields of view, corresponding to a smear slide area of 6.28 mm^2 following the method described by Backman and Shackleton (1983) and Rio et al. (1990). Relative abundance, expressed in percentage, and absolute abundance, expressed as number of specimens per 10 mm^2 in the slides, were calculated. Only one sample is completely barren and few samples in the lower part of the core, mainly corresponding to the ice-rafted debris (IRD) deposits, contain very rare nannofossils. The state of coccolith preservation varies from poor to good. A number of ecological indices were calculated and considered for environmental reconstruction, such as:

- the ratio between *Emiliania huxleyi* and *Coccolithus pelagicus* s.l. (H/P ratio) that in the Nordic Seas fossil assemblages gives indication on the location of the Arctic Front (Andruleit and Baumann, 1998) separating the seasonally sea ice covered Polar and Arctic water from the warmer and saltier Atlantic-derived water. This ratio was expressed in logarithmic scale;

Table 2
Radiocarbon dates and calendar year calibrations for core 17603-3 record.

Lab. code	Depth (cm)	Material	^{14}C age	Age error	1 σ cal age (cal a BP)	2 σ cal age (cal a BP)	Median probability (cal a BP)
OS-123791	0	*N. pachyderma* sin	720	20	257–336 and 344–356	151–159 and 227–424	302
OS-123804	20	*N. pachyderma* sin	2280	35	1745–1873	1686–1938	1813
OS-123796	80	*N. pachyderma* sin	4590	35	4654–4663 and 4673–4807	4569–4832	4723
OS-123408	140	*N. pachyderma* sin	6520	50	6851–7027	6787–7129	6946
OS-123536	160	*N. pachyderma* sin	6840	35	7250–7357	7201–7408	7303
OS-123786	210	Mix planktonic foraminifera	7750	40	8054–8200	8010–8281	8143
OS-123409	360	Mix planktonic foraminifera	8770	60	9299–9450	9199–9509	9370
OS-123657	660	*N. pachyderma* sin	10,900	40	12,221–12,476	12,085–12,539	12,335
OS-123411	820	Mix planktonic foraminifera	12,400	120	13,652–13,957	13,495–14,083	13,800
OS-123425	970	Mix planktonic foraminifera	12,850	170	14,126–14,802	13,957–15,125	14,505

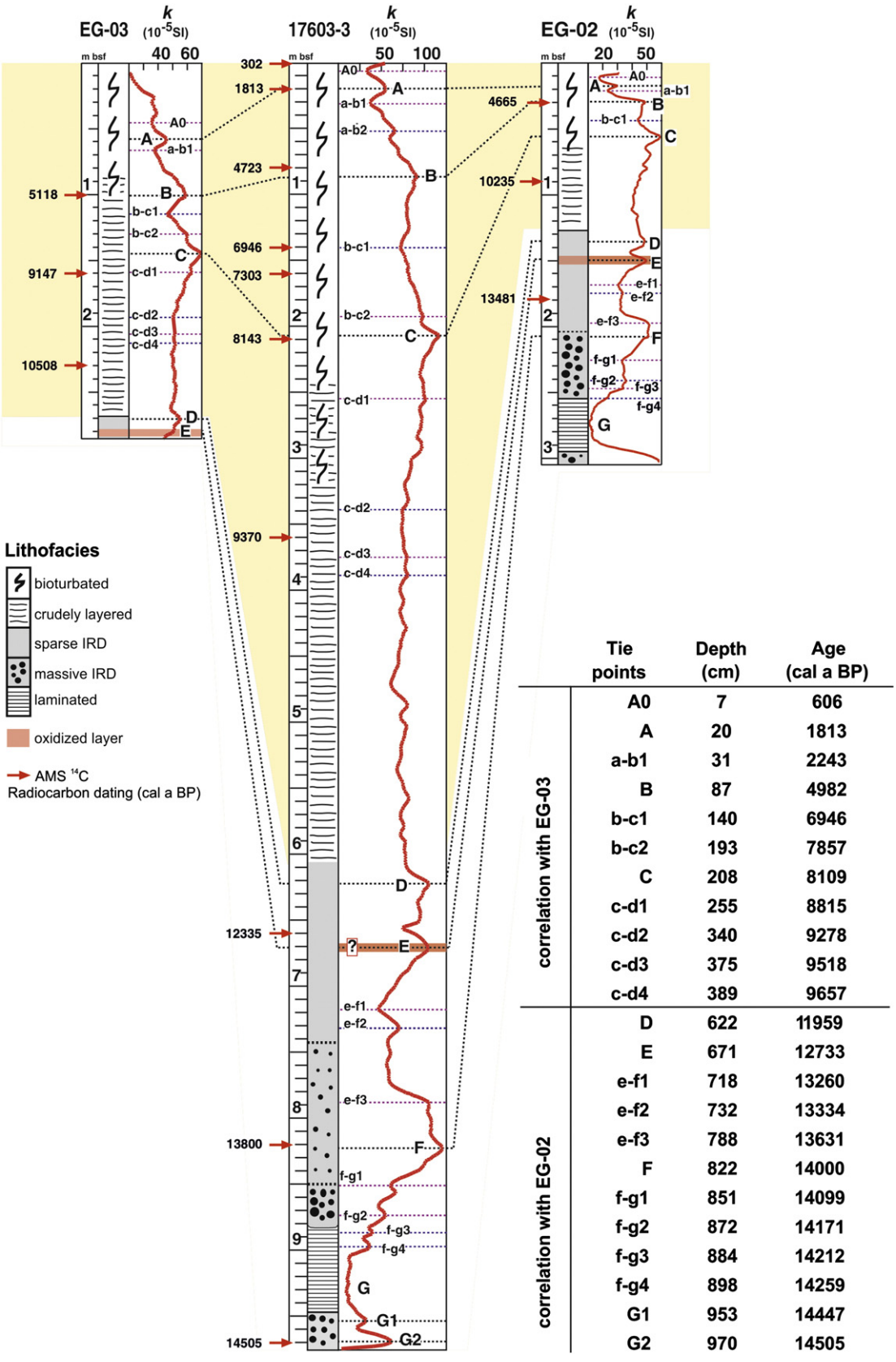

	Tie points	Depth (cm)	Age (cal a BP)
correlation with EG-03	A0	7	606
	A	20	1813
	a-b1	31	2243
	B	87	4982
	b-c1	140	6946
	b-c2	193	7857
	C	208	8109
	c-d1	255	8815
	c-d2	340	9278
	c-d3	375	9518
	c-d4	389	9657
correlation with EG-02	D	622	11959
	E	671	12733
	e-f1	718	13260
	e-f2	732	13334
	e-f3	788	13631
	F	822	14000
	f-g1	851	14099
	f-g2	872	14171
	f-g3	884	14212
	f-g4	898	14259
	G1	953	14447
	G2	970	14505

Fig. 2. Correlation between 17603-3, EG-02 and EG-03 cores, based on the proposed age model (see text for details). Calibrated calendar ages are indicated with red arrows.

- the dominance and Shannon Wiener diversity indices were calculated from species relative abundance, using the software PAST (Hammer et al., 2001).

Additionally, the cold-water taxa, obtained by the sum of the *C. pelagicus* s.l., *E. huxleyi* (>4 μm) and *Gephyrocapsa muellerae*, were plotted against warm-water taxa that includes *E. huxleyi* (<4 μm), *Gephyrocapsa oceanica* and small *Gephyrocapsa* spp.

3.3.2. Diatoms

A total of 48 samples were analysed for diatom content at a variable spacing distance of 10–20 cm. Slides for diatoms were prepared following the technique described by Rathburn et al. (1997). At least 300 diatom valves were identified in each sample and counted at 1000× magnification using an Ortholux light microscope following the method described by Crosta and Koç (2007). In the samples containing rare diatoms, in terms of numbers, the counting was extended to 1000 fields of view. Relative abundance, expressed in percentage, and total absolute diatom abundance (ADA), expressed as number of frustules per gram of dry weight (v/gdw), were calculated for each sample using the methodology described by Armand (1997). The dominance and Shannon Wiener diversity indices were calculated from species relative abundance, using the software PAST (Hammer et al., 2001).

3.3.3. Planktonic foraminifera

The 51 samples analysed for planktonic foraminifera were dry weighed and wet sieved at 63 μm, keeping the silt-clay fraction for mineralogical analysis. The sandy residues were dried at 50 °C, weighed and dry-sieved at 150 μm. Only the latter fraction (>150 μm) was analysed, for comparison with the results obtained from the sediment cores recovered in the area surrounding site 17603-3 (i.e. Lucchi et al., 2013). About 250 specimens were counted for each sample and identified at species level; subsequently relative abundance of each species was expressed as relative percentage. The taxonomy follows that of Hemleben et al. (1989) and Darling et al. (2006). The flux of planktonic foraminiferal assemblage (planktonic foraminiferal accumulation rate - PFAR) (number/cm^2/kyr) was determined together with the flux of the three dominant species *Neogloboquadrina pachyderma* (s), *Turborotalita quinqueloba* and *Neogloboquadrina incompta* as:

$$\text{Species AR} = \text{Abundance of planktonic foraminifera per g of dry sediment } (\text{n}\cdot\text{g}^{-1}) \cdot \text{dry bulk density } (\text{g}\cdot\text{cm}^{-3}) \cdot \text{sedimentation rate } \left(\text{cm}\cdot\text{ka}^{-1}\right).$$

In addition, the number of planktonic foraminiferal fragments was counted and expressed as the relative percentage of the total planktonic foraminiferal abundance to quantify the degree of dissolution according to Thunell (1976) and Conan et al. (2002). The dominance and Shannon diversity indices were calculated from species relative abundance, using the software PAST (Hammer et al., 2001).

4. Results

The age model for the studied core and the comparison with the sedimentary sequence of the neighbouring core EG-02, indicate the presence of an expanded sequence spanning last 14.5 cal ky BP (974 cm-thick, instead of 305 cm of core EG-02, Fig. 2). In particular, the Holocene sequence appears exceptionally expanded with over 600 cm with respect to the 250 cm of core EG-03 and many other cores collected in this area (e.g. Jessen et al., 2010 and references therein).

4.1. Lithology and sediment characteristics

The sedimentary sequence (Fig. 3) from the bottom to the top of the core consists of ice-rafted debris (IRD)-rich sediments and finely laminated sediments, containing cm/mm-thick sandy or silty layers (974–880 cm). The interval 880–605 cm contains sparse IRD that are abundant between 835 and 880 cm. Sandy/silty mottles and crudely layered sediments (605–240 cm) contain abundant black patches composed of organic matter rich sediments (vigorous reaction to peroxide water). The interval 240–0 cm consists of bioturbated sediments.

The grain size distribution (Fig. 3) is characterized by predominant silt, often over 60% with an almost constant clay content (ca. 22% on average), and little sand content (10% on average). Peaks of sand correspond to the sandy layers of the laminated facies (e.g. at 940 cm), whereas slightly higher contents characterize the crudely layered lithofacies.

The water content increases progressively from bottom to the top of the core with minimum values corresponding to sandy layers.

The predominant clay mineral is illite (43–66%), followed by kaolinite (12–31%), chlorite (14–23%) and smectite (4–18%) (Fig. 3). Illite, chlorite and kaolinite have an almost stable percentage down core, except within the laminated sediments, where illite decreases having an opposite trend with respect to chlorite and kaolinite (slight increase of percentages). Smectite has an up-core general increasing trend, with low–trace values at the base of the core where laminated and IRD-rich sediments occur and consistently higher values in the crudely layered and heavily bioturbated sediments.

The Ca/Ti and Fe/Ti ratios (Fig. 3) were used to distinguish between biogenic and terrigenous input respectively. The two trends are almost opposite with biogenic-Ca barren sediments in the laminated and massive IRD lithofacies at the base of the core. The biogenic-Ca content increases progressively from 835 cm (14 cal ka BP) to the top of the core. At about 660 cm (12.3 cal ka BP) there is a distinct relative increase of the Fe content (minimum of Ca content), corresponding to a peak of the magnetic susceptibility that, in other cores, has been related to the presence of an oxidized layer (OX1, Lucchi et al., 2013), not observed in the studied core.

4.2. Micropalaeontological content

4.2.1. Calcareous nannofossils

The following taxa are discussed: *Calcidiscus leptoporus*, *Coccolithus pelagicus* s.l., *Emiliania huxleyi, Gephyrocapsa muellerae*, *Gephyrocapsa oceanica*; *Gephyrocapsa* <3 μm are indicated as small *Gephyrocapsa* spp. The assemblage is well represented by Holocene species together with some Palaeogene and Cretaceous reworked taxa (*Discoaster binodosus*, *Arkhangelskiella maastrichtiana*, *Biscutum* spp., *Staurolithites* spp., *Eiffellithus* spp., *Microrhabdulus* spp., *Tranolithus* spp., *Watznaueria* spp., *Zeugrhabdotus* spp.). For most micropalaeontological studies, the presence of reworked specimens is usually considered as a disturbing factor where palaeoenvironmental and biostratigraphic interpretations are to be made. However, reworking of microfossils, such as calcareous nannofossils, can be used providing useful information on erosion-transport processes acting in the area (Ferreira et al., 2008). Chiefly on the basis of biometric subdivisions, the following *E. huxleyi* morphotypes were distinguished: *E. huxleyi* <4 μm and *E. huxleyi* > 4 μm, following Colmenero-Hidalgo et al. (2002). The *E. huxleyi* <4 μm variety shows warm-water preferences, whereas the *E. huxleyi* > 4 μm variety is considered to represent a cold-water form (Colmenero-Hidalgo et al., 2002; Flores et al., 2010). The nannofossil total abundance (without reworking), calculated on number of specimens per fixed area, spans from 0 to 11,476 coccoliths/10 mm^2 through the core (Fig. 4). The interval from 974 to 596 cm is characterized by low total abundance of nannofossils (up to 1331 coccoliths/10 mm^2), with predominant *E. huxleyi* (up to 1293 coccoliths/10 mm^2 or 100%) (Fig. 4). The increase of the relatively cold-water species *G. muellerae* (up

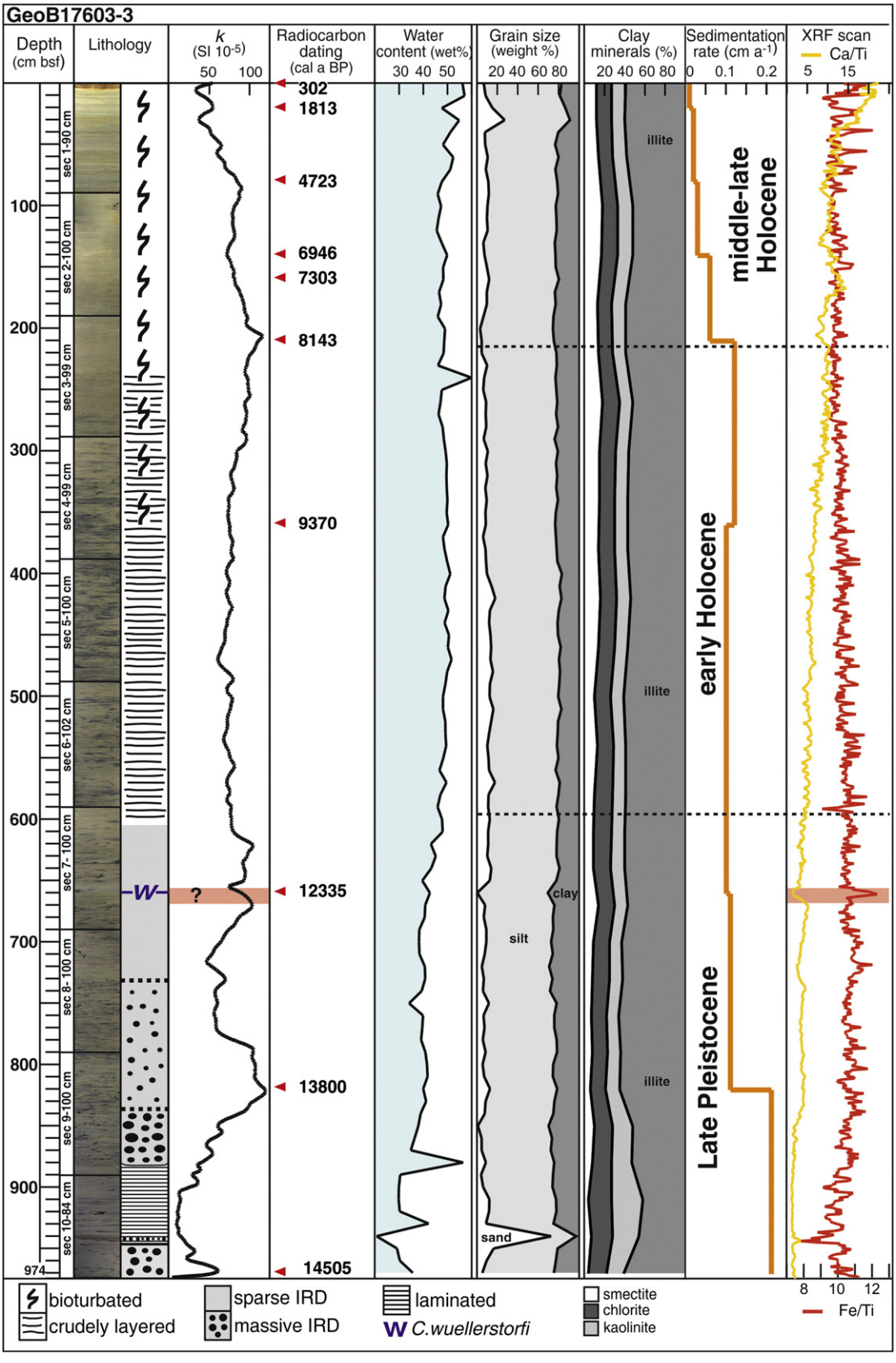

Fig. 3. Lithological log of core 17603-3 showing magnetic susceptibility (κ), water content, grain sizes, clay mineral content, sedimentation rate, Ca/Fe and Ca/Ti plots against core depth. The radiocarbon dated levels are also indicated. W = *Cibicides wuellerstorfi* first occurrence. The horizontal dotted lines correspond to time interval limits, commented in the discussions.

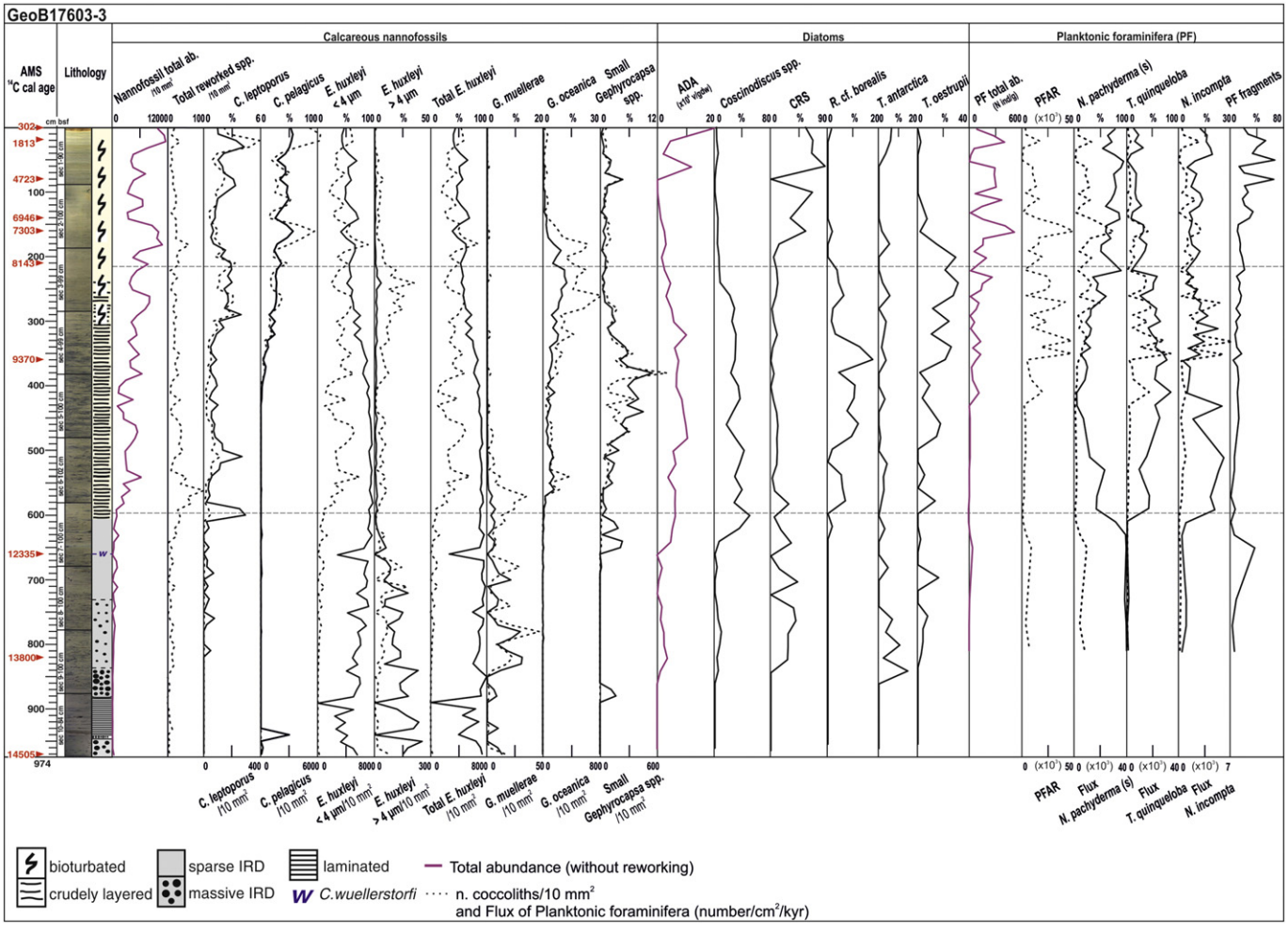

Fig. 4. Abundances of calcareous nannofossil, diatom and planktonic foraminiferal species for the investigated core plotted versus depth. ADA = absolute diatom abundance; CRS = *Chaetoceros* resting spore; W = *Cibicides wuellerstorfi* first occurrence; PF = planktonic foraminifera; PFAR = planktonic foraminiferal accumulation rate; microfossil total abundances are shown in purple. Red arrows indicate calibrated calendar ages dated by AMS ^{14}C (see Table 2 for details). Dotted lines indicate nannofossil absolute abundance, expressed as n. of coccoliths/10 mm^2 in the slide, and flux of planktonic foraminifera, expressed as number/cm^2/kyr.

to 12.39%) characterizes this interval along with a slight increase of total reworking (Fig. 4). A distinct crossover in abundance between *E. huxleyi* (>4 µm) and *E. huxleyi* (<4 µm) occurs between 650 and 630 cm (Fig. 4). The interval from 596 to 215 cm is characterized by increase of the total abundance of nannofossils (up to 8014 coccoliths/10 mm^2). The total reworking reaches values up to 97 coccoliths/10 mm^2 at 560 cm and it decreases towards the top of the core (Fig. 4). The interval between 596 and 215 cm is dominated by *E. huxleyi* (up to 94%) together with *C. leptoporus* (up to 4%), *G. oceanica* (up to 13%) and small *Gephyrocapsa* spp. (up to 11%) (Fig. 4). A drop of cold-water species *G. muellerae* (up to 0.5%) and a rise of relatively warm-water taxa *G. oceanica* (up to 6%) and small *Gephyrocapsa* spp. (up to 3%) occur at 560 cm (Fig. 4). A main crossover between dominance and diversity indices occurs at 410 cm (Fig. 5). An abrupt increase of relatively cold-water species *C. pelagicus* s.l. up to 36.04% and a concomitant slight decrease of *E. huxleyi* up to 53.49% occur between 390 and 215 cm (Fig. 4). The highest *G. oceanica* percentage is recorded at 240 cm with values up to 12.54% (Fig. 4). The interval between 215 and 0 cm is characterized by high values of *C. pelagicus* s.l. (up to 56.63%) and *E. huxleyi* (up to 69.11%). *Gephyrocapsa oceanica* records an abrupt decrease together with a general nannofossil total abundance drop (up to 3210 coccoliths/10 mm^2); although small *Gephyrocapsa* spp. relative abundance is generally low, its abundance trend shows a peak above 4% at 80 cm. The nannofossil total abundance increases to its highest value (11,476 coccoliths/10 mm^2) and it is persistently high up to the top of the core (Fig. 4).

Since the nannofossil assemblage is of low diversity through the core (Shannon Wiener diversity index up to 1.56), important changes in the assemblage structure can be described by ratio variations of the two dominant species *E. huxleyi* and *C. pelagicus* s.l. (H/P ratio), following Andruleit and Baumann (1998) (Fig. 5). According to recent oceanographic settings in the Nordic Seas an H/P ratio of >0 is indicative of Atlantic influenced conditions, while an H/P ratio of <0 indicates Arctic to Polar influenced conditions. The H/P ratio spans from −0.16 to 3.14 through the core (Fig. 5). An abrupt H/P ratio decrease is shown within the interlaminated lithofacies at 940 cm (up to 0); the highest H/P ratio is recorded between 460 and 450 cm with values up to 3.14. The H/P ratio presents a descending trend towards the top of the core (Fig. 5).

4.2.2. Diatoms

Seventeen diatom genera and 33 species were recognized. The absolute diatom abundance (ADA) spans from 0 to 23.3 × 10^6 v/gdw. The interval from 974 to 840 cm is characterized by the total absence of diatoms. The first diatom appearance occurs at 840 cm. The ADA shows values between 0 and 7.4 × 10^6 v/gdw from 840 to 596 cm. *Chaetoceros* (subgenus *Hyalochaete*) resting spore (CRS) dominates the assemblage reaching relative abundances up to 42.9%; the slight

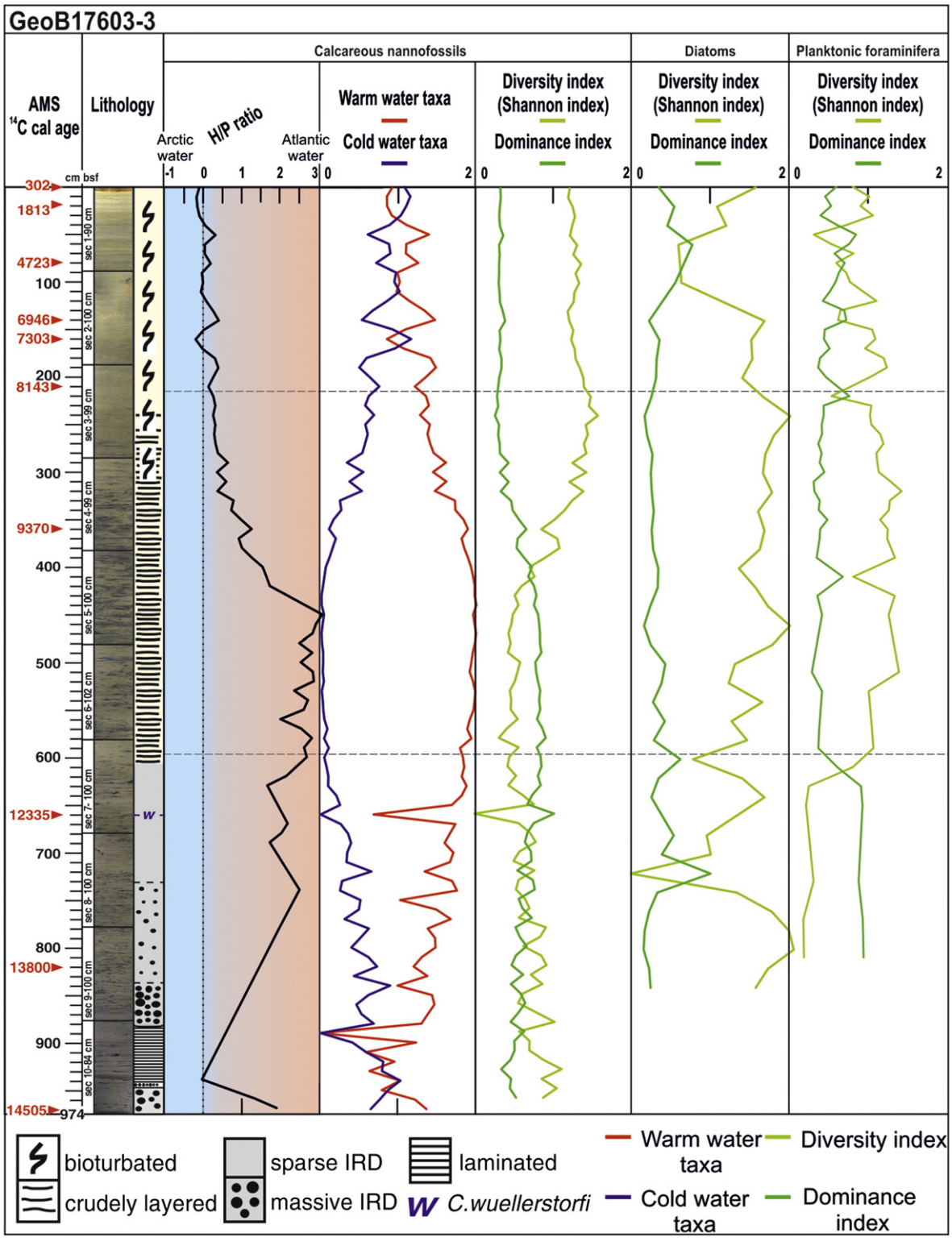

Fig. 5. Various ecological indices plotted against depth. The ratio of the two nannofossil dominant species *Emiliania huxleyi* and *Coccolithus pelagicus* (H/P ratio) equal to 0, approximately, marks the transition from Atlantic to Arctic influenced conditions. The cold-water taxa group (*C. pelagicus*, *E. huxleyi* (>4 μm) and *Gephyrocapsa muellerae*) are plotted against warm-water taxa (*E. huxleyi* (<4 μm), *Gephyrocapsa oceanica* and small *Gephyrocapsa* spp.). Dominance and Shannon Wiener diversity indices for all microfossil groups are shown. W = *Cibicides wuellerstorfi* first occurrence. Calibrated calendar ages are indicated with red arrows.

increase of relatively warm-water taxa *Coscinodiscus* spp. (up to 75%) and *Thalassiosira oestrupii* (up to 14%) characterizes the interval between 840 and 596 cm along with three peaks of the cold-water species *Thalassiosira antarctica*. The latter presents a descending trend towards the top of this interval with the highest peak at 840 cm (14%) (Fig. 4). The interval from 596 to 215 cm is characterized by the decrease of CRS and the abrupt increase of ADA, associated to high relative abundance of warm-water species *Coscinodiscus* spp. (mainly *C. marginatus* and *C. radiatus*). This genus reaches values up to 63% between 596 and 215 cm and slightly decreases towards the top of this interval.

Rhizosolenia cf. *borealis*, proxy for mixing water, derived from warmer (Norwegian) and colder (Arctic) waters, occurs between 596 and 215 cm. A peak of *T. oestrupii* abundance (28%) is recorded at 240 cm. Although *T. antarctica* relative abundance is generally very low, its abundance trend shows a peak above 5% at 260 cm. The ADA presents two main peaks at 480 cm (12.4×10^6 v/gdw) and at 320 cm (11.9×10^6 v/gdw). The interval from 215 to 0 cm is characterized by an abrupt increase of CRS (up to 87.1%). *Coscinodiscus* spp. and *T. oestrupii* show values up to ~6% until 140 cm, then they abruptly decrease to 0%. Generally low ADA ($0.2–3.6 \times 10^6$ v/gdw) is recorded until 80 cm. Diatoms disappear abruptly around 80 cm (Fig. 4). *Coscinodiscus* spp. is the only warm-water taxa in the upper part of the core having relative abundance above 2%. The cold-water related species *T. antarctica* increases in the topmost 40 cm of the core showing values up to 6%. The ADA abruptly increases in the uppermost 80 cm reaching the highest value (23.3×10^6 v/gdw) at the top of the core (Fig. 4). Shannon Wiener diversity index spans from 0 to 2.04 and it is generally higher than dominance (0.16–1) (Fig. 5).

4.2.3. Planktonic foraminifera

The dominant planktonic foraminiferal species are *Neogloboquadrina pachyderma* (s), followed by *Turborotalita quinqueloba* and *Neogloboquadrina incompta*. *Globigerina bulloides*, *Globigerina falconensis*, *Globigerinita glutinata*, *Globigerinita uvula* and *Orcadia riedeli* are present in low percentages (<19%). In this paper, we considered only the dominant species as they represent >80% of the entire association and they are the most significant taxa for palaeoenvironmental interpretations. Planktonic foraminifera are rare or absent from the base of the core up to 410 cm and the total abundance shows an increasing trend towards the top of the core, reaching values higher than 500 ind/g of dry sediment (Fig. 4). The PFAR shows a slight decrease between 410 and 215 cm, it rises between 215 and 160 cm, reaching its highest value (about 50,000 ind/cm^2/ky) at 160 cm; in the upper part of the core, between 160 and 0 cm it drops to value lower than 20,000 ind/cm^2/ky. In the interval from 974 to 596 cm, *Neogloboquadrina pachyderma* (s) is the dominant species, but always with low abundance; its flux reaches the value of 8765 ind/cm^2/ky at the 650 cm (Fig. 4). A drastic reduction of *N. pachyderma* (s) both as percentage and as flux occurs between 596 and 410 cm and following, until 215 cm, again a rise with percentages exceeding 86% (Fig. 4). *Turborotalita quinqueloba* is the second most common species. In the lower part of the core it is virtually absent up to 596 cm. It is present with high percentages (22–81%) between 596 and 215 cm, and then it decreases in the upper part of the core (215–0 cm) up to 7%. The flux of *T. quinqueloba* shows low values until 420 cm (0–2064 ind/cm^2/ky) and it reaches its highest value (32,520 ind/cm^2/ky) at 350 cm. *Neogloboquadrina incompta* is found in very low percentages between 974 and 596 cm. It follows an increase up to 430 cm reaching percentages of 20–25%, with a decrease up to 8% at 450 cm. From 410 to 215 cm it increases with a maximum of 22% at 310 cm. In the upper part of the core (215–0 cm) *N. incompta* occurs with low percentages (up to 19%) (Fig. 4). The percentages of fragmented tests are high (up to 35%) between 974 and 596 cm and they span from 0 to 20% between 596 and 215 cm. In the upper part of the core (215–0 cm), the percentages of fragments show an increasing trend, reaching values of 32% at 130 cm (Fig. 4). Two main crossovers between dominance and Shannon diversity indices occur at 610 cm and 220 cm; other minor fluctuations are recorded towards the top of the core (Fig. 5).

5. Discussions

The recovered core contains an expanded sedimentary sequence that includes continuous Upper Pleistocene and Holocene sediments. The climatic fluctuations within the studied intervals are well depicted by the microfossil assemblages and distribution of smectite that, in the studied area, is mainly transported by the North Atlantic Current (Junttila et al., 2010). On the basis of the age model and variations in microfossil assemblages, three intervals of significant climate changes during the last 14.5 cal ky BP are identified: Late Pleistocene (14.5–11.7 cal ka BP; 974–596 cm), early Holocene (11.7–8.2 cal ka BP; 596–215 cm) and middle-late Holocene (8.2–0.3 cal ka BP; 215–0 cm).

5.1. Late Pleistocene: 14.5–11.7 cal ka BP (974–596 cm)

The oldest recognized sediments, at the base of the core, deposited between 14.5 and 11.7 cal ka BP. It includes the Bølling-Allerød interstadial (B-A, 14.5–12.9 cal ka BP; Kienast and McKay, 2001) and the Younger Dryas stadial (YD, 12.9–11.7 cal ka BP; Broecker et al., 2010), correlated with δ^{18}O record of the Greenland GRIP ice core (Johnsen et al., 1997) (Fig. 6). During the Late Pleistocene, the Svalbard/Barents Sea Ice Sheet (SBSIS) melting and retreat, forced by the seasonal contrast in insolation, influenced climate changes (Anderson et al., 1988), contributing to trigger the deglacial two-step dynamic (Alley et al., 1997; Broecker et al., 1985). The rare occurrence of nannofossils, diatoms and planktonic foraminifera in the lowermost part of core 17603-3 (Fig. 6) is related to low productivity as a result of sea-ice cover (Villa et al., 2005; Zamelczyk et al., 2012). In particular, the scarcity of calcareous nannofossils was primarily related to low sea surface temperature (SST) as well as the presence of large volume of dense sediment-laden meltwater, affecting light penetration during the initial phase of the deglaciation, dampening the primary productivity.

The laminated lithofacies, dating 14.4–14.2 cal ka BP, was interpreted as deriving from sediment-laden meltwater associated to the Meltwater Pulse 1A (MWP-1A) (Lucchi et al., 2013, 2015) (Fig. 6). The MWP-1A was responsible for massive input of terrigenous sediments in the depositional system as indicated also by the high sedimentation rate recorded during this interval (Fig. 3). According to Kienast et al. (2003) this event coincides with the Bølling warm interstadial. Lucchi et al. (2013) argued that this warm event was possibly characterized by multi-year sea ice on the basis of the scarcity of IRD content in the laminated sediments. In this scenario, the absence of diatoms between 14.5 and 14.1 cal ka BP could be related to the presence of turbid meltwaters and/or by dissolution due to the presence of aggressive stratified water masses.

The generally warming trend is depicted during the B-A through the increase of the *Emiliania huxleyi* and *Coccolithus pelagicus* s.l. ratio (H/P ratio) and progressive increase of smectite content, indicating enhanced advection of Atlantic water to the study area. Although low temperature water affinity (Braarud, 1979; Samtleben et al., 1995), the nannoplankton *C. pelagicus* s.l. preference for fronts of moderate salinity gradients (Cachão and Moita, 2000) is tentatively used to explain its rare occurrence during the Late Pleistocene deglaciation, responsible for freshwater release. Above the laminated sediments, the massive IRD interval (Fig. 3), dated between 14.2 and 14.0 cal ka BP according to our age model, indicates a sudden, massive increase of iceberg calving offshore the Kveithola Trough. According to Lucchi et al. (2013) this interval records one of the main SBSIS collapses that cleared the outer shelf area from permanent ice cover.

Following this ice-sheet collapse, the sedimentary sequence dated between 14.0 and 12.9 cal ka BP is characterized by the presence of cold-water taxa such as *Emiliania huxleyi* (>4 μm), *Gephyrocapsa muellerae* and *Thalassiosira antarctica* that suggest development of seasonal sea-ice. Freshwater released by iceberg melting, following the outer ice-sheet collapse, would result in increased sea-ice formation. As a matter of fact, present day observations from Southern high latitudes indicate that, while subsurface warm ocean current causes basal ice-shelf melting, freshwater around Antarctica, having a higher freezing point, caused the extension of the seasonal sea-ice over the past few years, despite increased temperatures (Collins et al., 2013; Turner and Overland, 2009). As confirmation of the analogy, a concurrent occurrence of the nannofossil *E. huxleyi* (<4 μm), and the diatoms *Coscinodiscus* spp. and *Thalassiosira oestrupii* suggests intrusion of

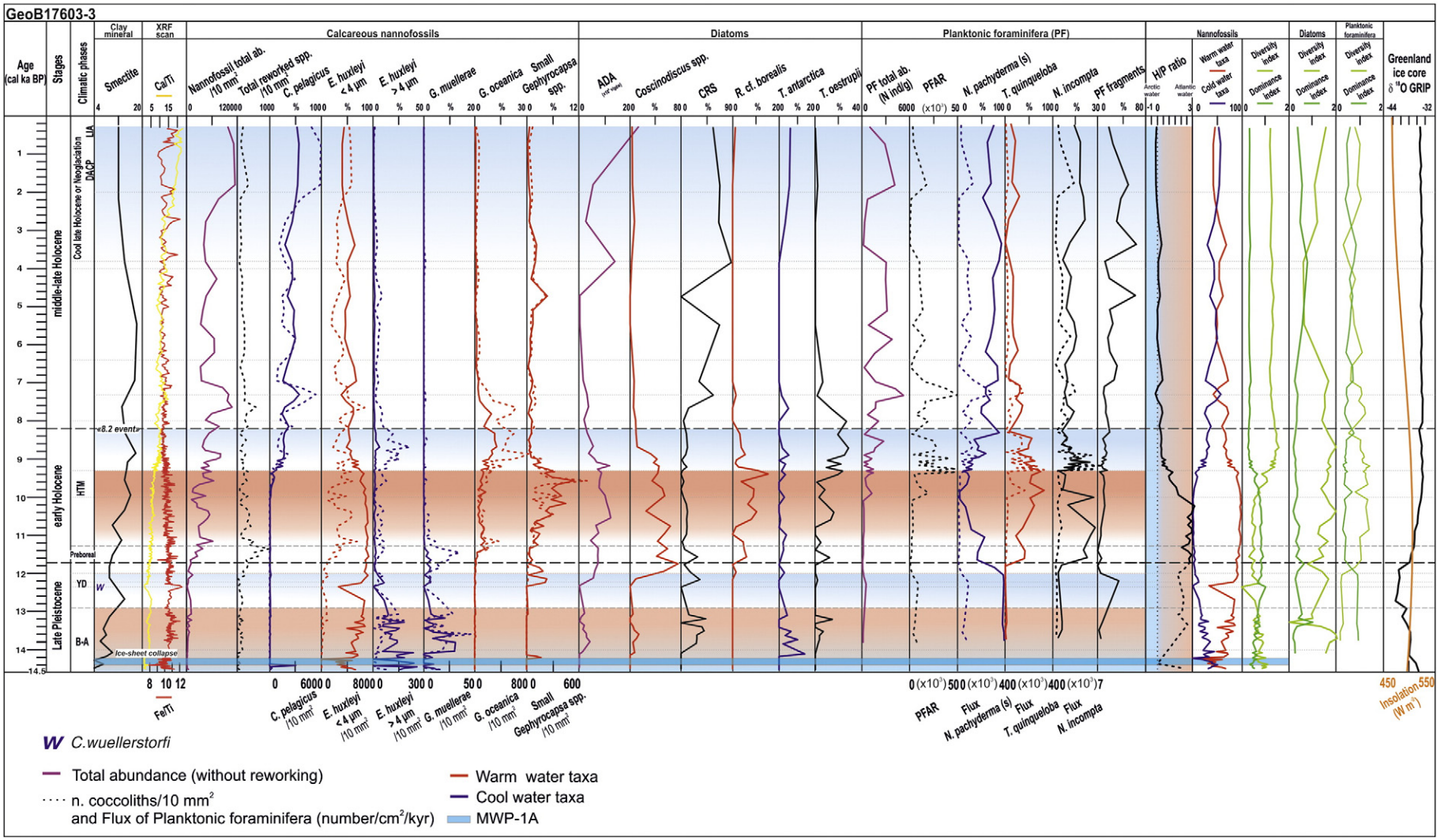

Fig. 6. Abundances of calcareous nannofossil, diatom and planktonic foraminiferal species for the investigated core plotted versus calendar age. Smectite and Ca/Fe, Ca/Ti ratio plots are shown. H/P ratio, warm and cold-water taxa curve, dominance and Shannon Wiener diversity are plotted versus calendar age. The lower part of the H/P ratio curve is dotted due to the absence of *C. pelagicus*, commented in the text. The summer insolation curve at 65° N for the studied interval, following Laskar et al. (2004), is shown in orange on the right of the figure. The Greenland ice core $\delta^{18}O$ GRIP and the summer insolation were selected and downloaded from official data repositories (e.g., International Research Institute for Climate and Society database, https://iridl.ldeo.columbia.edu/SOURCES/.ICE/.CORE/.GRIP/.o18/ and Virtual Observatory Paris Data Centre, http://vo.imcce.fr/insola/earth/online/earth/earth.html). ADA = absolute diatom abundance; CRS = *Chaetoceros* resting spore; W = *Cibicides wuellerstorfi* first occurrence; PF = planktonic foraminifera; PFAR = planktonic foraminiferal accumulation rate; MWP-1A = Meltwater Pulse 1A; B-A = Bølling-Allerød; YD = Younger Dryas; HTM = Holocene Thermal Maximum; DACP = Dark Ages Cold Period; LIA = Little Ice Age. Microfossil total abundances are shown in purple. Dotted lines indicate nannofossil absolute abundance, expressed as n. of coccoliths/10 mm^2 in the slide, and flux of planktonic foraminifera, expressed as number/cm^2/kyr.

relatively warm Atlantic water in the studied area. The absence of *Coccolithus pelagicus* s.l. and the decrease of *E. huxleyi* (>4 μm), *G. muellerae* and *T. antarctica* from 14.0 to 12.9 cal ka BP confirm the general climatic amelioration (B-A). Notably, the sharp decrease of *E. huxleyi* (>4 μm) confirms that this larger variety is a cold-water form (Colmenero-Hidalgo et al., 2002) whose abundance was reduced as a consequence of the progressive warming due to North Atlantic water during the B-A, supported also by the nannofossil cold-water and warm-water taxa curves, which indicate the climatic amelioration (Fig. 6). In addition, the presence of diatom *Chaetoceros* resting spores (CRS), between 14.1 and 12.9 cal ka BP, further indicates highly stratified and low salinity surface waters (Armand et al., 2005; Crosta et al., 1997), typical of intense melting during deglaciation conditions.

Between 12.9 and 11.7 cal ka BP the nannofossil, diatom and planktonic foraminiferal total abundances were generally low. In particular, between 12.9 and 12.2 cal ka BP, the neat decrease of the warm-water taxa *E. huxleyi* (<4 μm), the low abundance of *Coscinodiscus* spp. and the high planktonic foraminiferal fragmentation may indicate low SST. The concomitant presence of the cold-water taxa *Neogloboquadrina pachyderma* (s), *E. huxleyi* (>4 μm), *G. muellerae* and *T. antarctica* suggests evidences of a cold period that could correspond to the YD cold event, in agreement with Barron et al. (2009) who affirmed that microfossil proxies declined during the YD. The deterioration of the climate, during the interval 12.9–12.2 cal ka BP, is confirmed by the slight decrease of H/P ratio, indicating a Southern displacement of the Polar front (Andruleit and Baumann, 1998). Such conditions suggest an enhanced East Spitsbergen Current, which might have contributed to the inflow of polar waters in the Storfjorden-Kveithola. A possible re-advance of the ice sheet in the area is testified by a relative increase of Fe content in the sediments, representing the terrigenous component input with consequent reduction of the Ca content (Fig. 6).

The transition to warmer conditions, towards the end of the YD, was accompanied by enhanced biological productivity as reflected by the increase in the microfossil abundances at ca. 12 cal ka BP, the increase of Ca content and the regional first occurrence of the benthic foraminifer *Cibicidoides wuellerstorfi* (12.3 cal ka BP), defined as the first warming signal of bottom waters after the YD by T.L. Rasmussen et al. (2007) and Sarnthein et al. (2003).

5.2. Early Holocene: 11.7–8.2 cal ka BP (596–215 cm)

The interval between 11.7 and 8.2 cal ka BP includes the *Pre-Boreal Oscillation* (11.7–11.3 cal ka BP, Björck et al., 1997; T.L. Rasmussen et al., 2007; S.O. Rasmussen et al., 2007)) and the *Holocene Thermal Maximum* (HTM), also indicated as *Altithermal* or *Hypsithermal* (Wanner et al., 2008). The *Pre-Boreal Oscillation* represents the transition from Late Pleistocene to early Holocene milder climatic conditions. This early interval of the Holocene is characterized by the deposition of crudely layered sediments (Fig. 3), having sedimentological characteristics that indicate deposition under the effect of bottom currents (Lucchi et al., 2013). During this climatic transition, the biological productivity recovered and determined a rapid increase of the foraminiferal biodiversity, with high percentages of subpolar taxa as *Turborotalita quinqueloba* and *Neogloboquadrina incompta* that are indicative of productive surface water masses found in the vicinity of the Arctic and Polar fronts (Fig. 6). The increase of Ca content, during this period, is correlated to calcareous nannofossil increasing trend. This rise indicates seasonal ice-free condition, as also supported by higher H/P ratio that marks the beginning of the interglacial conditions.

The peak of Cretaceous reworked coccoliths at 11.4 cal ka BP (Fig. 6) can be explained by resedimentation of Cretaceous sediments (Hjelle, 1993) eroded by ice streams during the previous deglaciation phase (Andreassen et al., 2008; Ottesen et al., 2008).

Following the *Pre-Boreal Oscillation*, a relatively warm stable climatic phase occurred (11.3–9.3 cal ka BP), characterized by a sharp increased abundance of calcareous nannofossils, dominated by *Emiliania huxleyi* (<4 μm), *Gephyrocapsa oceanica*, small *Gephyrocapsa* spp., along with the diatoms *Coscinodiscus* spp., *Thalassiosira oestrupii*, *Rhizosolenia* cf. *borealis*, that are warm-water taxa indicating a pronounced inflow of warm Atlantic water into the study area. The increase of smectite supports this interpretation. The presence of *Coscinodiscus* spp. and *R.* cf. *borealis* among diatoms reflects shallowing of the mixed layer (Koç and Schrader, 1990) as a consequence of stronger summer insolation. The high flux of the planktonic foraminifer *N. incompta* confirms the climatic amelioration with strongly stratified water column, characterized by a reduced mixed layer and high chlorophyll-a concentrations (King and Howard, 2003). This climatic interval is defined as the HTM because the subsurface waters along the Western margin of Svalbard were dominated by Atlantic water reaching their maximum temperature (Jansen et al., 2009; Jessen et al., 2010; Kaufman et al., 2004; Rasmussen and Thomsen, 2014; Wanner et al., 2008). Our data are comparable with the diatom results observed in cores EG-02, EG-03 and SV-04, collected in the neighbouring Storfjorden TMF (Lucchi et al., 2013). The coccolith and diatom concentration peak, registered at ca. 10 cal ka BP, might reflect the response of the phytoplankton to the orbitally-forced maximum summer insolation (Laskar et al., 2004; Wanner et al., 2008), responsible for the HTM (Kaufman et al., 2004; Renssen et al., 2009, 2012). The H/P ratio supports the SST increase at around 10 cal ka BP, in agreement with the insolation curve (Laskar et al., 2004) (Fig. 6). Warm conditions are sustained also by the crossover between dominance and diversity indices of the nannofossil and planktonic foraminiferal assemblages (Fig. 6). Cronin and Cronin (2015) and Moran et al. (2006) asserted that the strengthening of warm inflowing Atlantic water in the Arctic is one of the mechanisms driving the species increasing diversity. According to Baumann et al. (2000) this warm environment determined the Northern displacement of the Arctic front.

A cooling trend, starting at approximately 9.3 cal ka BP, is marked by a relative increase of cold-water taxa, such as *Coccolithus pelagicus* s.l., *Thalassiosira antarctica* and *N. pachyderma* (s) (Fig. 6). The decrease of smectite values confirms a decline of Atlantic water inflow in the area, in agreement with a decrease of the H/P ratio. Evidence of climatic deterioration towards the top of the early Holocene is supported by reduction of warm-water taxa, as *E. huxleyi* (<4 μm), small *Gephyrocapsa* spp., *Coscinodiscus* spp., *R.* cf. *borealis, T. quinqueloba* and *N. incompta*, culminating in the so-called "8.2 event" (Alley et al., 1997). The latter event was hypothetically generated by a catastrophic release of freshwater from the glacial lakes Agassiz and Ojibway that drained cold-waters through the Hudson Strait after the Laurentide Ice Sheet collapse, affecting the North Atlantic Deep Water formation (Barber et al., 1999). According to Alley et al. (1997) this is considered to be the most noticeable climatic event of the Holocene recorded in the Greenland ice cores.

5.3. Middle-late Holocene: post 8.2–0.3 cal ka BP (215–0 cm)

The stratigraphic interval between 8.2 and 0.3 cal ka BP is characterized by bioturbated sediments (Fig. 3) that were deposited by contour currents under progressively ameliorated environmental conditions favourable to the biological productivity.

Starting from ca. 8 cal ka BP the calcareous microfossil abundances experienced a new increasing trend (Fig. 6). The peaks of *Coccolithus pelagicus* s.l. and CRS at 7.3 cal ka BP are not to be ascribed to high primary productivity, but rather to higher dissolution resistance of these species (Fig. 6).

The calcareous microfossil concentration increases during the interval 6.4–4 cal ka BP corresponding to a short period of reintensification of Atlantic Water advection, which maximum clearly occurred during the previous HTM. During this interval, the calcareous nannofossil association is characterized by shared relative abundances between cold and warm water-taxa.

A gradual cooling during the late Holocene, since ca. 4 cal ka BP, is recorded by nannofossil total abundance decrease together with the

increase of cold-water taxa as *Coccolithus pelagicus* s.l., *Neogloboquadrina pachyderma* (s) and *Thalassiosira antarctica*. This change indicates sea surface cooling with seasonal sea ice presence, in agreement with Ślubowska-Woldengen et al. (2008) who indicated that an atmospheric cooling and a reduction of the Atlantic water inflow occurred between 4 and 2 cal ka BP. The preference of *Gephyrocapsa muellerae*, a well-known cold-water adapted taxon (Bollmann, 1997), in this interval is not supported by our data. The highest CRS peak recorded at 3.8 cal ka BP indicates spring sea ice melting coinciding with the ADA peak (14×10^6 v/gdw). The cooling trend corresponds to the so-called Cool Late Holocene (Andersen et al., 2004) known also as Neoglacial cold event that was described by Koç et al. (1993) and attributed to the decline of summer insolation in the Northern high latitude by Imbrie et al. (1992) and Wanner et al. (2011).

According to our age model, the interval dating 2.5–2 cal ka BP is characterized by a crossover between warm and cold-water nannofossil taxa. However, the sampling resolution in the upper part of the core is too low to provide detailed information on very short climatic variation. A clear increase of the cold-water nannofossil taxa *C. pelagicus* s.l. marks a climatic deterioration since ca. 2 cal ka BP that we related to the Dark Ages Cold Period (DACP; Ljungqvist, 2010). The latter and the following Little Ice Age (LIA) are thought to have been triggered by a combination of a reduction in solar irradiance and explosive volcanism (Wanner et al., 2011). The very last sample, dated at 0.3 cal ka BP, falls within the LIA time; the only micropalaeontological evidences that could suggest harsh LIA conditions are the high *C. pelagicus* s.l., *N. pachyderma* (s) and *T. antarctica* abundances. The increasing trend of the nannofossil cold-water taxa curve supports the Neoglaciation evidences towards the top of the core (Fig. 6).

6. Conclusions

The 974 cm long sediment core collected from the Kveithola TMF middle slope (GeoB17603-3) contains an expanded sedimentary record dating 14.5–0.3 cal ka BP; over 600 cm deposited during the Holocene. Quantitative microfossil assemblage analyses (calcareous nannofossils, diatoms and planktonic foraminifera) and clay minerals gave promising results outlining their close relation to the climatically induced changes in the characteristics of surface water on the NW Barents Sea over last 14.5 cal ky BP. Accordingly with previous studies in the region, we assigned the microfossil species to different palaeoecological groups, and in particular with respect to Sea Surface Temperature (SST). Nannofossil indices such as *E. huxleyi* and *C. pelagicus* s.l. (H/P) ratio, poorly used in the Arctic environment, is considered in support of major climatic variations. The reconstructions of surface water conditions highlight the strong coupling between the advances and retreats of the Svalbard-Barents Sea Ice Sheet (SBSIS), the interplay of Atlantic/Arctic water masses flows over the study area, and insolation orbital forcing.

Three intervals of significant climate change were identified: Late Pleistocene (14.5–11.7 cal ka BP; 974–596 cm), early Holocene (11.7–8.2 cal ka BP; 596–215 cm) and middle-late Holocene (8.2–0.3 cal ka BP; 215–0 cm):

- Late Pleistocene sediments (14.5–11.7 cal ka BP) record a) the Bølling-Allerød interstadial, consisting of laminated lithofacies, indicating intense ice-melting, and massive IRD deposition that accompanied the SBSIS collapse; and b) the Younger Dryas stadial, characterized by a general decrease of microfossils abundance with presence of cold taxa and often fragmented/reworked species.
- The transition to warmer conditions, during the late YD is indicated by the increase in microfossil abundances and the first occurrence of the benthic foraminifer *Cibicidoides wuellerstorfi* as proxy for Atlantic influx and climatic amelioration. According to calibrated radiocarbon ages the first occurrence of *C. wuellerstorfi* dates as early as 12.3 cal ka BP.
- The early Holocene interval (11.7–8.2 cal ka BP) records a) the Pre-Boreal Oscillation, characterized by a progressive increase of microfossils biodiversity and abundance, with high H/P ratio marking the onset of interglacial condition; and b) the Holocene Thermal Maximum (HTM) characterized by a sharp increase of microfossil abundance (warm-water taxa), Ca and smectite contents. The high concentration of coccoliths and diatoms observed at ca. 10 cal ka BP has been related to the phytoplankton response to the orbitally-forced maximum summer insolation, responsible for the HTM. From approximately 9.3 cal ka BP, an environmental cooling trend is depicted on the microfossils assemblage and the H/P ratio, culminating at around 8.2 cal ka BP;
- The middle-late Holocene is characterized by an initial (8.2–4.0 cal ka BP) environmental amelioration, characterized by a slight dominance of warm taxa, after which another gradual cooling is recorded by the increase of cold-water adapted taxa that we associated to the decline of summer insolation in the Northern high latitude, responsible for the onset of the Neoglacial cold event.

Acknowledgements

The authors acknowledge the Captain, crew, and scientific party of the CORIBAR cruise onboard the German R/V Maria S. Merian (Tromsø, 15 July–Tromsø, 15 August 2013). In particular, we acknowledge T.J.J. Hanebuth as chief scientist during the cruise and H. Landzik for organizing the sampling party and the preliminary analyses (Radiographs, and Multi sensor core logger) at MARUM laboratories. We thank S. Miserocchi of the CNR-ISMAR Bologna (Italy) for the help given during the XRF core-scan analysis. Special thanks are also addressed to M. Rebesco and D. Accettella that kindly contributed with bathymetric data and G.A. Prista for scientific discussion and suggestions that greatly improved the manuscript. We would like to acknowledge B. Trummel of Polar Educators International for critically reading the manuscript and for valuable comments. We thank the Editor and the reviewers for their worthy comments on the manuscript. This study was supported by the PNRA project CORIBAR-IT (PNRA PdR C2/2013), the Italian project Premiale ARCA, and the Spanish project DEGLABAR (CTM2010-17386).

References

Aagaard, K., Foldvik, A., Hillman, S., 1987. The West Spitsbergen Current: disposition and water mass transformation. J. Geophys. 92, 3778. http://dx.doi.org/10.1029/JC092iC04p03778.

Alley, R.B., Mayewski, P.A., Sowers, T., Stuiver, M., Taylor, K.C., Clark, P.A., 1997. Holocene climate variability: a prominent widespread event 8200 years ago. Geology 25, 483–486. http://dx.doi.org/10.1130/0091-7613(1997)025<0483:HCIAPW>2.3.CO;2.

Andersen, C., Koç, N., Jennings, A., Andrews, J.T., 2004. Nonuniform response of the major surface currents in the Nordic Seas to insolation forcing: implications for the Holocene climate variability. Paleoceanography 19, 1–16. http://dx.doi.org/10.1029/2002PA000873.

Anderson, C.W., Barnosky, P.J., Bardein, P.J., Behling, L., Brubaker, E.J., Cushing, J., Dodson, B., Dworetsky, P.J., Guetter, S.P., Harrison, B., Huntley, J.E., Kutzbach, V., Markgraf, R., Marvel, M.S., McGlone, A., Mix, N.T., Moar, J., Morley, R.A., Perrottn, G.M., Peterson, W.L., Prell, I.C., Prentice, J.C., Ritchie, N., Roberts, W., Ruddiman, F., Salinger, M.J., Spaulding, W.G., Street-Perrott, F.A., Thompson, R.S., Wang, P.K., Webb III, T., Winer, M.G., Wright, H.E., 1988. Climatic changes of the last 18,000 years: observations and model simulations. Science 241 (4869), 1043–1052.

Andreassen, K., Laberg, J.S., Vorren, T.O., 2008. Seafloor geomorphology of the SW Barents Sea and its glacidynamic implications. Geomorphology 97, 157–177.

Andruleit, H.A., Baumann, K.H., 1998. History of the Last Deglaciation and Holocene in the Nordic seas as revealed by coccolithophore assemblages. Mar. Micropaleontol. 35, 179–201. http://dx.doi.org/10.1016/S0377-8398(98)00021-8.

Armand, L., 1997. The Use of Diatom Transfer Functions in Estimating Sea-surface Temperature and Sea-ice in Cores from the Southeast Indian Ocean (Ph.D. Thesis) Australian National University, Canberra.

Armand, L.K., Crosta, X., Romero, O., Pichon, J.J., 2005. The biogeography of major diatom taxa in Southern Ocean sediments: 1. Sea ice related species. Palaeogeogr. Palaeoclimatol. Palaeoecol. 223, 93–126. http://dx.doi.org/10.1016/j.palaeo.2005.02.015.

Backman, J., Shackleton, N.J., 1983. Quantitative biochronology of Pliocene and early Pleistocene calcareous nannofossils from the Atlantic, Indian and Pacific oceans. Mar. Micropaleontol. 8, 141–170. http://dx.doi.org/10.1016/0377-8398(83)90009-9.

Backman, J., Fornaciari, E., Rio, D., 2009. Biochronology and paleoceanography of late Pleistocene and Holocene calcareous nannofossil abundances across the Arctic Basin. Mar. Micropaleontol. 72, 86–98. http://dx.doi.org/10.1016/j.marmicro.2009.04.001.

Barber, D.C., Dyke, A., Hillaire-Marcel, C., Jennings, A.E., Andrews, J.T., Kerwin, M.W., Bilodeau, B., McNeely, R., Southon, J., Morehead, M.D., Gagnon, J.-M., 1999. Forcing of the cold event of 8,200 years ago by catastrophic drainage of Laurentide lakes. Nature 400, 344–348. http://dx.doi.org/10.1038/22504.

Barron, J.A., Bukry, D., Dean, W.E., Addison, J.A., Finney, B., 2009. Paleoceanography of the Gulf of Alaska during the past 15,000 years: results from diatoms, silicoflagellates, and geochemistry. Mar. Micropaleontol. 72, 176–195. http://dx.doi.org/10.1016/j.marmicro.2009.04.006.

Baumann, K.H., Andruleit, H., Samtleben, C., 2000. Coccolithophores in the Nordic Seas: comparison of living communities with surface sediment assemblages. Deep. Res. Part II Top. Stud. Oceanogr. 47, 1743–1772. http://dx.doi.org/10.1016/S0967-0645(00)00005-9.

Biscaye, P.E., 1965. Mineralogy and sedimentation of recent deep-sea clay in the Atlantic Ocean and adjacent seas and oceans. Geol. Soc. Am. Bull. 76, 803–832. http://dx.doi.org/10.1130/0016-7606(1965)76[803:masord]2.0.co;2.

Björck, S., Rundgren, M., Ingólfsson, Ó., Funder, S., 1997. The Preboreal oscillation around the Nordic Seas: terrestrial and lacustrine responses. J. Quat. Sci. 12, 455–465. http://dx.doi.org/10.1002/(SICI)1099-1417(199711/12)12:6<455::AID-JQS316>3.0.CO;2-S.

Blindheim, J., Rey, F., 2004. Water-mass formation and distribution in the Nordic Seas during the 1990s. ICES J. Mar. Sci. 61, 846–863. http://dx.doi.org/10.1016/j.icesjms.2004.05.003.

Bollmann, J., 1997. Morphology and biogeography of *Gephyrocapsa* coccoliths in Holocene sediments. Science 29 (80-.), 319–350. http://dx.doi.org/10.1016/S0377-8398(96)00028-X.

Bown, P.R., Young, J.R., 1998. Calcareous Nannofossil Biostratigraphy. Chapman-Hall, Dordrecht, The Netherlands.

Braarud, T., 1979. The temperature range of the non-motile stage of *Coccolithus pelagicus* in the North Atlantic region. Br. Phycol. J. 14, 349–352.

Broecker, W.S., Peteet, D.M., Rind, D., 1985. Does the ocean-atmosphere system have more than one stable mode of operation? Nature 315, 21–26. http://dx.doi.org/10.1038/315021a0.

Broecker, W.S., Denton, G.H., Edwards, R.L., Cheng, H., Alley, R.B., Putnam, A.E., 2010. Putting the Younger Dryas cold event into context. Quat. Sci. Rev. 29, 1078–1081. http://dx.doi.org/10.1016/j.quascirev.2010.02.019.

Cachão, M., Moita, M.T., 2000. *Coccolithus pelagicus*, a productivity proxy related to moderate fronts off Western Iberia. Mar. Micropaleontol. 39, 131–155. http://dx.doi.org/10.1016/S0377-8398(00)00018-9.

Collins, M., Knutti, R., Arblaster, J., Dufresne, J.-L., Fichefet, T., Friedlingstein, P., Gao, X., Gutowski, W.J., Johns, T., Krinner, G., Shongwe, M., Tebaldi, C., Weaver, A.J., Wehner, M., 2013. Long-term climate change: projections, commitments and irreversibility. Clim. Chang. 2013 Phys. Sci. Basis. Contrib. Work. Gr. I to Fifth Assess. Rep. Intergov. Panel Clim. Chang., pp. 1029–1136. http://dx.doi.org/10.1017/CBO9781107415324.024.

Colmenero-Hidalgo, E., Flores, J.A., Sierro, F.J., 2002. Biometry of *Emiliania huxleyi* and its biostratigraphic significance in the Eastern North Atlantic Ocean and Western Mediterranean Sea in the last 20 000 years. Mar. Micropaleontol. 46, 247–263.

Conan, S.M.H., Ivanova, E.M., Brummer, G.J.A., 2002. Quantifying carbonate dissolution and calibration of foraminiferal dissolution indices in the Somali Basin. Mar. Geol. 182, 325–349. http://dx.doi.org/10.1016/S0025-3227(01)00238-9.

Cronin, T.M., Cronin, M.A., 2015. Biological response to climate change in the Arctic Ocean: the view from the past. Arktos 1, 4. http://dx.doi.org/10.1007/s41063-015-0019-3.

Crosta, X., Koç, N., 2007. Chapter eight diatoms: from micropaleontology to isotope geochemistry. Dev. Mar. Geol. http://dx.doi.org/10.1016/S1572-5480(07)01013-5.

Crosta, X., Pichon, J.J., Labracherie, M., 1997. Distribution of Chaetoceros resting spores in modern peri-Antarctic sediments. Mar. Micropaleontol. 29, 283–299. http://dx.doi.org/10.1016/S0377-8398(96)00033-3.

Damiani, D., Giorgetti, G., Turbanti, I.M., 2006. Clay mineral fluctuations and surface textural analysis of quartz grains in Pliocene-Quaternary marine sediments from Wilkes Land continental rise (East-Antarctica): paleoenvironmental significance. Mar. Geol. 226, 281–295. http://dx.doi.org/10.1016/j.margeo.2005.11.002.

Darling, K.F., Kucera, M., Kroon, D., Wade, C.M., 2006. A resolution for the coiling direction paradox in *Neogloboquadrina pachyderma*. Paleoceanography 21. http://dx.doi.org/10.1029/2005PA001189.

Ferreira, J., Cachão, M., González, R., 2008. Reworked calcareous nannofossils as ocean dynamic tracers: the Guadiana shelf case study (SW Iberia). Estuar. Coast. Shelf Sci. 79, 59–70. http://dx.doi.org/10.1016/j.ecss.2008.03.012.

Flores, J.A., Colmenero-Hidalgo, E., Mejía-Molina, A.E., Baumann, K.H., Henderiks, J., Larsson, C., Prabhu, C., Sierro, F.J., Rodrigues, T., 2010. Distribution of large *Emiliania huxleyi* in the Central and Northeast Atlantic as a tracer of surface ocean dynamics during the last 25,000 years. Mar. Micropaleontol. 76, 53–66.

Friedman, G.M., Sanders, J.E., 1978. Principles of Sedimentology. John Wiley, New York.

Groot, D.E., Aagaard-Sørensen, S., Husum, K., 2014. Reconstruction of Atlantic water variability during the Holocene in the western Barents Sea. Clim. Past 10, 51–62. http://dx.doi.org/10.5194/cp-10-51-2014.

Hammer, Ø., Harper, D.A.T., Ryan, P.D., 2001. PAST: palaeontological statistics software package for education and data analysis. Palaeontol. Electron. 4, 1–9. http://dx.doi.org/10.1163/001121611X566785.

Hemleben, C., Spindler, M., Anderson, O.R., 1989. Modern Planktonic Foraminifera. Springer.

Hjelle, A., 1993. The Geology of Svalbard: Oslo. Norsk Polarinstitutt (163 pp.).

Imbrie, J., Boyle, E.A., Clemens, S.C., Duffy, A., Howard, W.R., Kukla, G., Kutzbach, J., Martinson, D.G., McIntyre, A., Mix, A.C., Molfino, B., Morley, J.J., Peterson, L.C., Pisias, N.G., Prell, W.L., Raymo, M.E., Shackleton, N.J., Toggweiler, J.R., 1992. On the structure and origin of major glaciation cycles 1. Linear responses to Milankovitch forcing. Paleoceanography 7, 701–738. http://dx.doi.org/10.1029/92pa02253.

Jansen, E., Andersson, C., Moros, M., Nisancioglu, K.H., Nyland, B.F., Telford, R.J., 2009. The early to mid-Holocene thermal optimum in the North Atlantic. Nat. Clim. Var. Glob. Warm. A Holocene Perspect. 123–137 http://dx.doi.org/10.1002/9781444300932.ch5.

Jessen, S.P., Rasmussen, T.L., Nielsen, T., Solheim, A., 2010. A new Late Weichselian and Holocene marine chronology for the western Svalbard slope 30,000–0 cal years BP. Quat. Sci. Rev. 29, 1301–1312. http://dx.doi.org/10.1016/j.quascirev.2010.02.020.

Johnsen, S.J., Clausen, H.B., Dansgaard, W., Gundestrup, N.S., Hammer, C.U., Andersen, U., Andersen, K.K., Hvidberg, C.S., Dahl-Jensen, D., Steffensen, J.P., Shoji, H., Sveinbjörnsdóttir, Á.E., White, J., Jouzel, J., Fisher, D., 1997. A record along the Greenland Ice Core Project deep ice core and the problem of possible Eemian climatic instability. J. Geophys. Res. 102, 26397. http://dx.doi.org/10.1029/97JC00167.

Junttila, J., Aagaard-Sørensen, S., Husum, K., Hald, M., 2010. Late Glacial-Holocene clay minerals elucidating glacial history in the SW Barents Sea. Mar. Geol. 276, 71–85. http://dx.doi.org/10.1016/j.margeo.2010.07.009.

Kaufman, D.S., Ager, T.A., Anderson, N.J., Anderson, P.M., Andrews, J.T., Bartlein, P.J., Brubaker, L.B., Coats, L.L., Cwynar, L.C., Duvall, M.L., Dyke, A.S., Edwards, M.E., Eisner, W.R., Gajewski, K., Geirsdottir, A., Hu, F.S., Jennings, A.E., Kaplan, M.R., Kerwin, M.W., Lozhkin, A.V., MacDonald, G.M., Miller, G.H., Mock, C.J., Oswald, W.W., Otto-Bliesner, B.L., Porinchu, D.F., Rhland, K., Smol, J.P., Steig, E.J., Wolfe, B.B., 2004. Holocene thermal maximum in the western Arctic (0–180°W). Quat. Sci. Rev. 23, 529–560. http://dx.doi.org/10.1016/j.quascirev.2003.09.007.

Kienast, S.S., McKay, J.L., 2001. Sea-surface Temperature Reconstruction of Sediment Core JT96-09PC. http://dx.doi.org/10.1594/PANGAEA.738484.

Kienast, M., Hanebuth, T.J.J., Pelejero, C., Steinke, S., 2003. Synchroneity of meltwater pulse 1a and the Bølling warming: new evidence from the South China Sea. Geology 31, 67–70. http://dx.doi.org/10.1130/0091-7613(2003)031<0067:SOMPAT>2.0.CO;2.

King, A., Howard, W.L., 2003. Planktonic foraminiferal flux seasonality in Subantarctic sediment traps: a test for paleoclimate reconstructions. Paleoceanography 18, 1–17. http://dx.doi.org/10.1029/2002PA000839.

Koç, N., Schrader, H., 1990. Surface sediment diatom distribution and Holocene paleotemperature variations in the Greenland, Iceland and Norwegian Sea. Paleoceanography 5, 557–580. http://dx.doi.org/10.1029/PA005i004p00557.

Koç, N., Jansen, E., Haflidason, H., 1993. Paleoceanographic reconstructions of surface ocean conditions in the Greenland, Iceland and Norwegian seas through the last 14 ka based on diatoms. Quat. Sci. Rev. 12, 115–140. http://dx.doi.org/10.1016/0277-3791(93)90012-B.

Laskar, J., Robutel, P., Joutel, F., Gastineau, M., Correia, C.M., Levrard, B., 2004. Astrophysics a long-term numerical solution for the insolation. Astronomy 285, 261–285. http://dx.doi.org/10.1051/0004-6361.

Ljungqvist, F.C., 2010. A new reconstruction of temperature variability in the extra-tropical northern hemisphere during the last two millennia. Geogr. Ann. Ser. A Phys. Geogr. 92, 339–351. http://dx.doi.org/10.1111/j.1468-0459.2010.00399.x.

Loeng, H., 1991. Features of the physical oceanographic conditions of the Barents Sea. Polar Res. 10, 5–18. http://dx.doi.org/10.1111/j.1751-8369.1991.tb00630.x.

Lucchi, R.G., Camerlenghi, A., Rebesco, M., Colmenero-Hidalgo, E., Sierro, F.J., Sagnotti, L., Urgeles, R., Melis, R., Morigi, C., Bàrcena, M.A., Giorgetti, G., Villa, G., Persico, D., Flores, J.A., Rigual-Hernandez, A.S., Pedrosa, M.T., Macri, P., Caburlotto, A., 2013. Post-glacial sedimentary processes on the Storfjorden and Kveithola trough mouth fans: significance of extreme glacimarine sedimentation. Glob. Planet. Chang. 111, 309–326. http://dx.doi.org/10.1016/j.gloplacha.2013.10.008.

Lucchi, R.G., Sagnotti, L., Camerlenghi, A., Macrì, P., Rebesco, M., Pedrosa, M.T., Giorgetti, G., 2015. Marine sedimentary record of Meltwater Pulse 1a along the NW Barents Sea continental margin. Arktos 1, 7. http://dx.doi.org/10.1007/s41063-015-0008-6.

Mangerud, J., Gulliksen, S., 1975. Apparent radiocarbon ages of recent marine shells from Norway, Spitsbergen, and Arctic Canada. Quat. Res. 5, 263–273. http://dx.doi.org/10.1016/0033-5894(75)90028-9.

Mangerud, J., Bondevik, S., Gulliksen, S., Karin Hufthammer, A., Høisæter, T., 2006. Marine ^{14}C reservoir ages for 19th century whales and molluscs from the North Atlantic. Quat. Sci. Rev. 25, 3228–3245. http://dx.doi.org/10.1016/j.quascirev.2006.03.010.

Moran, K., Backman, J., Brinkhuis, H., Clemens, S.C., Cronin, T., Dickens, G.R., Eynaud, F., Gattacceca, J., Jakobsson, M., Jordan, R.W., Kaminski, M., King, J., Koc, N., Krylov, A., Martinez, N., Matthiessen, J., McInroy, D., Moore, T.C., Onodera, J., O'Regan, M., Pälike, H., Rea, B., Rio, D., Sakamoto, T., Smith, D.C., Stein, R., St John, K., Suto, I., Suzuki, N., Takahashi, K., Watanabe, M., Yamamoto, M., Farrell, J., Frank, M., Kubik, P., Jokat, W., Kristoffersen, Y., 2006. The Cenozoic palaeoenvironment of the Arctic Ocean. Nature 441, 601–605. http://dx.doi.org/10.1038/nature04800.

Ottesen, D., Stokes, C.R., Rise, L., Olsen, L., 2008. Ice-sheet dynamics and ice streaming along the coastal parts of northern Norway. Quat. Sci. Rev. 27, 922–940. http://dx.doi.org/10.1016/j.quascirev.2008.01.014.

Rasmussen, T.L., Thomsen, E., 2014. Brine formation in relation to climate changes and ice retreat during the last 15,000 years in Storfjorden, Svalbard, 76–78 N. Paleoceanography 29, 911–929. http://dx.doi.org/10.1002/2014PA002643.

Rasmussen, T.L., Thomsen, E., Ślubowska, M.A., Jessen, S., Solheim, A., Koç, N., 2007a. Paleoceanographic evolution of the SW Svalbard margin (76°N) since 20,000 ^{14}C yr BP. Quat. Res. 67, 100–114. http://dx.doi.org/10.1016/j.yqres.2006.07.002.

Rasmussen, S.O., Vinther, B.M., Clausen, H.B., Andersen, K.K., 2007b. Early Holocene climate oscillations recorded in three Greenland ice cores. Quat. Sci. Rev. 26, 1907–1914. http://dx.doi.org/10.1016/j.quascirev.2007.06.015.

Rathburn, A.E., Pichon, J.J., Ayress, M.A., De Deckker, P., 1997. Microfossil and stable-isotope evidence for changes in Late Holocene palaeoproductivity and palaeoceanographic

conditions in the Prydz Bay region of Antarctica. Palaeogeogr. Palaeoclimatol. Palaeoecol. 131, 485–510. http://dx.doi.org/10.1016/S0031-0182(97)00017-5.
Rebesco, M., Liu, Y., Camerlenghi, A., Winsborrow, M., Laberg, J.S., Caburlotto, A., Diviacco, P., Accettella, D., Sauli, C., Wardell, N., Tomini, I., 2011. Deglaciation of the western margin of the Barents Sea Ice Sheet - a swath bathymetric and sub-bottom seismic study from the Kveithola Trough. Mar. Geol. 279, 141–147. http://dx.doi.org/10.1016/j.margeo.2010.10.018.
Reimer, P., 2013. IntCal13 and Marine13 radiocarbon age calibration curves 0–50,000 years cal BP. Radiocarbon 55, 1869–1887. http://dx.doi.org/10.2458/azu_js_rc.55.16947.
Renssen, H., Seppä, H., Heiri, O., Roche, D.M., Goosse, H., Fichefet, T., 2009. The spatial and temporal complexity of the Holocene thermal maximum. Nat. Geosci. 2, 411–414. http://dx.doi.org/10.1038/ngeo513.
Renssen, H., Seppä, H., Crosta, X., Goosse, H., Roche, D.M., 2012. Global characterization of the Holocene Thermal Maximum. Quat. Sci. Rev. 48, 7–19. http://dx.doi.org/10.1016/j.quascirev.2012.05.022.
Rio, D., Raffi, I., Villa, G., 1990. Pliocene-Pleistocene calcareous nannofossil distribution patterns in the western Mediterranean. Proc., Sci. results, ODP, Leg 107. Tyrrhenian Sea 107, 513–533.
Rüther, D.C., Bjarnadóttir, L.R., Junttila, J., Husum, K., Rasmussen, T.L., Lucchi, R.G., Andreassen, K., 2012. Pattern and timing of the northwestern Barents Sea Ice Sheet deglaciation and indications of episodic Holocene deposition. Boreas 41, 494–512. http://dx.doi.org/10.1111/j.1502-3885.2011.00244.x.
Sagnotti, L., Macrì, P., Lucchi, R., Rebesco, M., Camerlenghi, A., 2011. A Holocene paleosecular variation record from the northwestern Barents Sea continental margin. Geochem. Geophys. Geosyst. 12, 1–24. http://dx.doi.org/10.1029/2011GC003810.
Samtleben, C., Schäfer, P., Andruleit, H., Baumann, A., Baumann, K.-H., Kohly, A., Matthiessen, J., Schro¨der-Ritzrau, A., Synpal Working Group, 1995. Plankton in the Norwegian– Greenland Sea: from living communities to sediment assemblages — an actualistic approach. Geol. Rundsch. 84, 108–136.
Sarnthein, M., Van Kreveld, S., Erlenkeuser, H., Grootes, P.M., Kucera, M., Pflauman, U., Schulz, M., 2003. Centennial-to-millennial-scale periodicities of Holocene climate and sediment injections off the western Barents shelf, 75°N. Boreas 32, 447–461. http://dx.doi.org/10.1111/j.1502-3885.2003.tb01227.x.
Ślubowska-Woldengen, M., Koç, N., Rasmussen, T.L., Klitgaard-Kristensen, D., Hald, M., Jennings, A.E., 2008. Time-slice reconstructions of ocean circulation changes on the continental shelf in the Nordic and Barents Seas during the last 16,000 cal yr B.P. Quat. Sci. Rev. 27, 1476–1492. http://dx.doi.org/10.1016/j.quascirev.2008.04.015.
Stuiver, M., Reimer, P.J., 1993. Extended ^{14}C data base and revised CALIB 3.0 ^{14}C age calibration program. Radiocarbon 35, 215–230.
Svendsen, J.I., Alexanderson, H., Astakhov, V.I., Demidov, I., Dowdeswell, J.A., Funder, S., Gataullin, V., Henriksen, M., Hjort, C., Houmark-Nielsen, M., Hubberten, H.W., Inglfsson, I., Jakobsson, M., Kjr, K.H., Larsen, E., Lokrantz, H., Lunkka, J.P., Lysa, A., Mangerud, J., Matiouchkov, A., Murray, A., Moller, P., Niessen, F., Nikolskaya, O., Polyak, L., Saarnisto, M., Siegert, C., Siegert, M.J., Spielhagen, R.F., Stein, R., 2004. Late Quaternary ice sheet history of northern Eurasia. Quat. Sci. Rev. 1229–1271 http://dx.doi.org/10.1016/j.quascirev.2003.12.008.
Thunell, R.C., 1976. Optimum indices of calcium carbonate dissolution, in deep-sea sediments. Geology 4, 525–528. http://dx.doi.org/10.1130/0091-7613(1976)4<525:OIOCCD>2.0.CO;2.
Turner, J., Overland, J., 2009. Contrasting climate change in the two polar regions. Polar Res. 28, 146–164. http://dx.doi.org/10.1111/j.1751-8369.2009.00128.x.
Villa, G., Palandri, S., Wise, S.W., 2005. Quaternary calcareous nannofossils from Periantarctic basins: paleoecological and paleoclimatic implications. Mar. Micropaleontol. 56, 103–121. http://dx.doi.org/10.1016/j.marmicro.2005.03.006.
Wanner, H., Beer, J., Bütikofer, J., Crowley, T.J., Cubasch, U., Flückiger, J., Goosse, H., Grosjean, M., Joos, F., Kaplan, J.O., Küttel, M., Müller, S.A., Prentice, I.C., Solomina, O., Stocker, T.F., Tarasov, P., Wagner, M., Widmann, M., 2008. Mid- to Late Holocene climate change: an overview. Quat. Sci. Rev. 27, 1791–1828. http://dx.doi.org/10.1016/j.quascirev.2008.06.013.
Wanner, H., Solomina, O., Grosjean, M., Ritz, S.P., Jetel, M., 2011. Structure and origin of Holocene cold events. Quat. Sci. Rev. 30, 3109–3123. http://dx.doi.org/10.1016/j.quascirev.2011.07.010.
Winsborrow, M.C.M., Andreassen, K., Corner, G.D., Laberg, J.S., 2010. Deglaciation of a marine-based ice sheet: Late Weichselian palaeo-ice dynamics and retreat in the southern Barents Sea reconstructed from onshore and offshore glacial geomorphology. Quat. Sci. Rev. 29, 424–442. http://dx.doi.org/10.1016/j.quascirev.2009.10.001.
Wollenburg, J.E., Kuhnt, W., 2000. The response of benthic foraminifers to carbon flux and primary production in the Arctic Ocean. Mar. Micropaleontol. 40 (3), 189–231. http://dx.doi.org/10.1016/S0377-8398(00)00039-6.
Zamelczyk, K., Rasmussen, T.L., Husum, K., Haflidason, H., de Vernal, A., Ravna, E.K., Hald, M., Hillaire-Marcel, C., 2012. Paleoceanographic changes and calcium carbonate dissolution in the central Fram Strait during the last 20 ka. Quat. Res. 78, 405–416. http://dx.doi.org/10.1016/j.yqres.2012.07.006.